International Journal of Thermal Sciences 188 (2023) 108245

Contents lists available at ScienceDirect

International Journal of Thermal Sciences

journal homepage: www.elsevier.com/locate/ijts

Rapid detection of the vacuum failure of logging tools based on the variation in equivalent thermal conductivity

Jiale Peng, Yujun Wang, Siqi Ding, Chao Deng, Fulong Wei, Xiaobing Luo *

School of Energy and Power Engineering, Huazhong University of Science and Technology, Wuhan, China

ARTICLE INFO

Keywords:
Rapid test method
Vacuum failure
Testing indicator
Equivalent thermal conductivity

ABSTRACT

The logging tool is the key downhole facility used for oil and gas exploration. A vacuum flask is indispensable for protecting the inside electronics of the logging tool from extreme working environments. During transport, assembly, or working processes, vacuum flask failure can lead to the destruction of the logging tool. The existing test methods are unable to detect vacuum failure quickly and accurately. To solve this problem, a rapid test method based on the variation in equivalent thermal conductivity before and after vacuum failure was proposed. First, the principle of this method was illustrated in detail, and a simplified 1D heat transfer model was calculated by the finite difference method. We found that the temperature rise ratio between the insulator and heat source (defined as P) can be used as the testing indicator with a 1 h testing time. Subsequently, a rapid test device was designed, and numerical simulations were performed to determine the critical values of the testing indicator for actual vacuum flasks. The simulated results showed that independent of the heating power and initial temperature, the P values for vacuum flasks in normal and abnormal states are 0.391 and 0.299, respectively, with a critical value of 0.351. Finally, experimental tests were conducted to test the effectiveness of the rapid test method and testing indicator. The experimental results showed that the measured P values of normal and abnormal vacuum flasks were above or below the critical value (Pe) under different test conditions, respectively, indicating that the proposed rapid test method can quickly and accurately detect vacuum failure. The maximum error between the simulated and experimental results was only 8.7%.

1. Introduction

As traditional shallow fields are depleted, the oil industry has been shifting its focus to ultradeep wells [1,2]. Previous studies have shown that the downhole temperature increases by 1–9 °C every 100 m in depth [3]. Therefore, in ultradeep wells, the downhole temperature commonly exceeds 200 °C [4]. Logging tools are applied to detect the distribution of oil and gas resources and thus inevitably work for several hours in extreme thermal environments [5]. However, limited by temperature resistance, the electronics inside the logging tool cannot operate continuously in such a high-temperature environment [6–8]. As a result, the petroleum industry typically applies various thermal management techniques to extend the tool's operating hours, such as active [9–20] and passive [21–27] thermal management techniques. Although the heat dissipation capability of passive thermal management is not as effective as that of active thermal management, it has been widely applied in the field of oil exploration due to its simple structure and high system reliability. The vacuum flask, which is used to insulate heat transfer from the external high-temperature environment, plays an irreplaceable role in the passive thermal management of logging tools [8]. The vacuum layer in the logging tool can significantly reduce the impact of the external high-temperature environment on the internal electronics by evacuation. However, the vacuum layer of the vacuum flask, sealed by welding, may sometimes fail during transport, assembly, or working processes.

There have been a large number of studies regarding vacuum failure. Dcmko et al. [28] experimentally investigated the change in heat transfer before and after vacuum failure in a high vacuum multilayer insulated pipeline, and the results showed that the heat flow in the radial direction of this insulated pipeline increased to 34 times that of the original one after vacuum failure. Bartcncv et al. [29] experimentally studied the heat transfer process of vacuum failure, and the results showed that the size of the breakout of the vacuum layer has no significant effect on the heat transfer, and once breakout occurs, the convective heat transfer and the heat transfer will rise sharply. By combining experiments and simulations, Xie et al. [30] obtained that

* Corresponding author.
E-mail address: luoxb@hust.edu.cn (X. Luo).

https://doi.org/10.1016/j.ijthermalsci.2023.108245
Received 22 November 2022; Received in revised form 9 January 2023; Accepted 16 February 2023

when helium intruded into the vacuum layer, its instantaneous heat flow was close to 600 W/m^2. Pomeroy et al. [31] concluded that there was a significant decrease in the static evaporation rate of liquid nitrogen in high vacuum multilayer tanks before and after vacuum failure. Zhu et al. [32] experimentally demonstrated the effect of leaking gas on the heat transfer process after vacuum failure and determined that helium possesses a larger heat flow value than air and nitrogen. Therefore, once the vacuum layer of the vacuum flask of the logging tool is destroyed, the thermal insulation performance is greatly reduced, and the temperature of the electronics quickly reaches the temperature limit. Even failure can occur during the next logging. Hence, to ensure that the logging tool works safely, the thermal insulation of the vacuum flask must be estimated quickly before the next logging.

At present, there are several test methods used to detect vacuum failure. In the first method, vacuum failure is determined by directly measuring the vacuum degrees [33]. In the second method, the evaporation rate is measured before and after vacuum failure. For example, Jurns et al. [34] conducted experiments on the heat transfer performance of buried cryogenic storage tanks after vacuum failure, and the results showed that the evaporation rate of cryogenic vessels after vacuum failure was 10 times higher than that before failure. The above two methods can quickly and directly test for vacuum failure. However, the vacuum valve must be reserved for connecting external equipment, but the vacuum flask of the logging tool, which is directly welded after vacuuming, cannot be connected to external equipment. Therefore, the above method is not applicable to vacuum failure detection of the logging tool. In the third method, vacuum failure is indirectly determined by measuring the heat transfer before and after the vacuum failure, without the need for a vacuum valve. For example, Wei et al. [35] proposed a new calorimeter to test the heat flow change before and after vacuum failure, but the test results are greatly influenced by the structure and shape of the calorimeter as well as the initial temperature. Wang et al. [36] characterized vacuum failure by detecting the temperature of the outer surface of the multilayer insulation material of liquid nitrogen tanks. However, the test results varied with the initial temperature, which did not have stable testing indicator. Since the initial temperature is uncertain for the logging tools, existing test methods for vacuum failure are not suitable for applications. Therefore, it is necessary to detect vacuum failure quickly and accurately, and the detected results should be stable and not change with the initial temperature.

In this paper, to tackle this persistent issue, a rapid test method based on the variation in equivalent thermal conductivity before and after vacuum failure is proposed. First, the fundamental principles of the rapid test method were presented in detail, and a simplified 1D heat transfer model inside the vacuum flask was calculated to find the testing indicator for judging vacuum failure. Subsequently, a rapid test device was designed, and numerical simulations were performed to determine the critical values of the test indicator for actual vacuum flasks. Finally, experimental tests were conducted to validate the effectiveness of the rapid test method.

2. Principles of the rapid test method

The vacuum flask of a logging tool is mainly composed of a metal shell and a vacuum layer. The vacuum layer, sealed by welding, has a vacuum degree greater than 10^{-2} Pa to reduce heat conduction as well as thermal convection. To further reduce the radiation heat leakage in the vacuum layer, a certain number of reflective screens are often added to the vacuum layer. Moreover, low-thermal-conductivity spacers are added between the reflective screens to prevent direct contact, thus reducing heat conduction. There are only two states of industrial vacuum flasks: the normal state and the vacuum failure state. In a normal vacuum flask, there is less thermal convection and heat conduction in the vacuum layer due to the evacuation process, and thermal radiation plays a dominant role in heat exchange. The vacuum layer of a normal vacuum flask can be equated to a solid layer with extremely low thermal conductivity. However, when the vacuum layer is broken, air will quickly enter the vacuum layer, and heat conduction and heat convection occupy the main position in heat exchange. The equivalent thermal conductivity of the vacuum layer of an abnormal vacuum flask can be considered a solid layer with a slightly higher thermal conductivity than that of air. By using the layer-by-layer model [37,38], the equivalent thermal conductivities of normal and failed vacuum flasks are calculated as 0.00014 W/(m^{-1}·K^{-1}) and 0.033 W/(m^{-1}·K^{-1}), respectively. Therefore, based on the change in equivalent thermal conductivity, vacuum failure can be determined by arranging the heat source and insulator through the temperature distribution in the vacuum flask.

Fig. 1(a) shows the heat transfer path of a normal vacuum flask. After the heat is generated from the heat source, only a slight amount of heat flows out from the circumferential direction due to the tremendous thermal resistance in the circumferential direction, and most of the heat is gathered and diffuses to the inner wall of the insulators in the vacuum flask. Fig. 1(b) shows the heat transfer path of an abnormal vacuum flask. After the heat is generated from the heat source, some of the heat leaks directly into the environment from the circumferential direction due to the small thermal resistance, and some of the heat still diffuses in the vacuum flask. Therefore, under the same conditions, different states of vacuum flasks possess different temperature distributions inside. In actual industrial applications, there is an urgent need to determine a stable testing indicator to quickly detect vacuum failure based on the thermal distribution of vacuum flasks in different states.

Therefore, the above heat transfer process of the rapid test method was simplified to obtain the criteria for judging the two states of the vacuum flask. The following reasonable assumptions were made.

1) The transient heat transfer for a single time step of the rapid test device can be solved as a quasi-static process.
2) The whole device is almost symmetrical in the axial and radial directions, which can be reduced to heat transfer between finite nodes in one dimension.
3) q is the equivalent of heat dissipation to the environment through the vacuum flask circumference, which can be expressed as [39]:

$$q = \frac{T - T_\infty}{R_{cir}} \tag{1}$$

where T represents the temperature of the internal point of the vacuum flask, T_∞ represents the external ambient temperature, and R_{cir} represents the circumferential for the equivalent thermal resistance of the vacuum flask from the internal heat source to the environment.

4) The heat source is equated to a point heat source. The heat capacity of the node at the heat source is equivalent to the sudden increase in sensible heat capacity due to the excessive power input at this location relative to the nodes at other locations.
5) The insulator possesses good thermal insulation and is regarded as adiabatic.
6) The contact thermal resistance between nodes and the variation in the physical properties of all materials with temperature are neglected.

Fig. 2 shows the 1D heat transfer model of the vacuum flask containing the internal heat source after simplification. The vacuum flask is axially divided into several unit nodes, which are classified into three types according to the characteristics of the nodes at different locations, and thermal conduction differential equations are established. Subsequently, based on the previous assumptions, the finite difference method is used to discretize the time and nodes, and the analysis of different types of nodes is as follows.

(1) Node at the middle

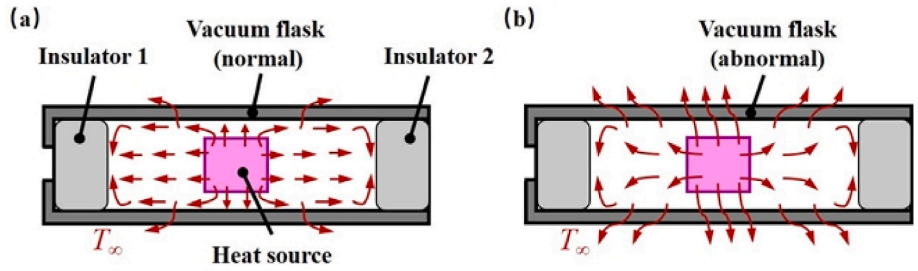

Fig. 1. Heat transfer path of the vacuum flask: (a) normal and (b) abnormal.

Fig. 2. The 1D heat transfer model of the vacuum flask containing the internal heat source after simplification.

There is heat conduction between the nodes at the middle and the nodes on both sides. At the same time, heat can be dissipated from the middle nodes to the outside. Therefore, the 1D unsteady thermal conduction differential equation with an internal heat source is applied as follows:

$$\rho c\frac{\partial T}{\partial t}=\lambda\frac{\partial^2 T}{\partial x^2}+\dot{q} \tag{2}$$

where ρ is the density of the material, c is the constant pressure specific heat capacity of the material, λ is the equivalent thermal conductivity of the material, T is the temperature, and $\dot{q}$ is the amount of heat dissipated per unit volume to the environment through the circumference of the vacuum flask, which can be expressed as

$$\dot{q}=\frac{(T-T_\infty)/R_{cir}\cdot(\Delta x\cdot 1\cdot 1)}{(\Delta x\cdot 1\cdot 1)}=\frac{T-T_\infty}{R_{cir}} \tag{3}$$

where Δx represents the node length.

Taking the forward difference for the nonstationary term and the intermediate difference for the diffusion term in Eq. (2), the following equation can be obtained.

$$T_m^{n+1}=\frac{\alpha(\Delta t)}{(\Delta x)^2}\left(T_{m+1}^n+T_{m-1}^n\right)+\left[1+\frac{\alpha(\Delta t)}{\lambda R_{cir}}-\frac{2\alpha(\Delta t)}{(\Delta x)^2}\right]T_m^n-\frac{\alpha(\Delta t)}{\lambda R_{cir}}T_\infty \tag{4}$$

where T_m^{n+1} is the temperature of the m_{th} node at the $(n+1)^{th}$ moment, T_{m+1}^n is the temperature of the $(m+1)^{th}$ node at the nth moment, and T_m^n is the temperature of the mth node at the nth moment. Δt is the calculated time step, and α is the thermal diffusion coefficient of the material,$\alpha = \lambda = \rho c$

The stability criterion is as follows.

$$\Delta t\le\frac{1}{\frac{2\alpha}{(\Delta x)^2}-\frac{\alpha}{\lambda R_{cir}}} \tag{5}$$

Eq. (5) illustrates that the time step must be limited to a certain range, which is related to the thermal diffusion coefficient, the thermal conductivity, the equivalent thermal resistance from the interior to the environment, and the length of the node.

(2) Node at the heat source

The internal heat source of the node at the heat source includes the heat input per unit volume and heat dissipation per unit volume to the environment through the circumference of the vacuum flask. The 1D unsteady thermal conduction differential equation can be expressed as follows:

$$\rho c_{eff}\frac{T_1^{n+1}-T_1^n}{\Delta t}=\lambda\frac{T_2^n-T_1^n}{(\Delta x)^2}+\frac{T_1^n-T_\infty}{R_{cir}}+\frac{Q}{\Delta x} \tag{6}$$

where T_1^{n+1} is the temperature of the 1st node at the $(n+1)^{th}$ moment, T_1^n is the temperature of the 1st node at the nth moment, T_2^n is the temperature of the 2nd node at the nth moment, and T_1 is the temperature of the heat source. Q represents the total energy input of the heat source. c_{eff} is the equivalent sensible heat capacity of the node at the heat source, which is calculated as follows:

$$c_{eff}=\frac{\rho_1 v_1 c_1+\rho_1 v_1 c_1}{\rho v} \tag{7}$$

where ρ_1, c_1, and v_1 represent the density, specific heat capacity, and volume of the metal parts at the heat source, respectively. ρ_2, c_2, and v_2 represent the density, specific heat capacity, and volume of the heat source, respectively.

Eq. (6) can be further transformed into

$$T_1^{n+1}=\frac{\alpha_{eff}(\Delta t)}{(\Delta x)^2}T_2^n+\left[1+\frac{\alpha_{eff}(\Delta t)}{\lambda R_{cir}}-\frac{\alpha_{eff}(\Delta t)}{(\Delta x)^2}\right]T_1^n-\frac{\alpha_{eff}(\Delta t)}{\lambda R_{cir}}T_\infty+\frac{\alpha_{eff}(\Delta t)}{\lambda(\Delta x)}Q \tag{8}$$

where α_{eff} represents the equivalent thermal diffusion coefficient of the node at the heat source.

The stability criterion is as follows:

$$\Delta t\le\frac{1}{\frac{\alpha_{eff}}{(\Delta x)^2}-\frac{\alpha_{eff}}{\lambda R_{cir}}} \tag{9}$$

(3) Node at the insulator

The node at the insulator absorbs the heat conduction from the previous node and dissipates heat to the environment in both circumferential and end directions. The discrete equation for the end node can be expressed as follows:

$$T_M^{n+1}=\frac{\alpha(\Delta t)}{(\Delta x)^2}T_{M-1}^n+\left[1+\frac{\alpha(\Delta t)}{\lambda R_{cir}}-\frac{2\alpha(\Delta t)}{(\Delta x)^2}\right]T_M^n-\frac{\alpha(\Delta t)}{\lambda R_{cir}}T_\infty \tag{10}$$

where M represents the last node, T_M^{n+1} is the temperature of the M^{th} node at the $(n+1)^{th}$ moment, T_M^n is the temperature of the M^{th} node at the nth moment, T_{M-1}^n is the temperature of the $(M\text{-}1)^{th}$ node at the nth moment, and T_M is the temperature of the insulator.

The stability criterion is the same as Eq. (5).

In the calculation, λ = 0.00014 W/(m-K) represents the case of normal conditions of the vacuum flask, and λ = 0.033 W/(m-K)

represents the case of vacuum failure of the vacuum flask, which is slightly higher than the equivalent thermal conductivity of air. The software MATLAB was used for performing 1D numerical simulations.

The temperature variation in the nodes in each part of the device with time can be obtained by using the above method. The nodes at the heat source and at the insulator are selected for analysis. Fig. 3 shows the temperature curves of these two nodes with an initial temperature of 20 °C and a heat source power of 20 W. Notably, the initial temperature is the same as the ambient temperature. The temperature at both nodes increases with time after heating. The temperature at the heat source rises faster, while the temperature at the insulator increases more slowly. The temperatures in the normal vacuum flask are significantly higher than those in the abnormal flask. After the vacuum layer is destroyed, the circumferential thermal resistance is reduced, a large amount of heat flow leaks from the circumferential direction, and less heat remains inside the vacuum flask, resulting in a lower internal temperature. This further shows that when the vacuum layer of the vacuum flask is broken, the temperature distribution will be significantly changed; thus, it can be used to determine the state of the vacuum flask.

For vacuum flask testing in actual industrial environments, it is difficult to maintain the initial temperature and heating power at different places. Therefore, the test results of the same state of the same vacuum flask cannot be affected by the initial temperature and heating power, which means that the testing indicator is independent of the initial temperature and power. Furthermore, to ensure the integration of the device, the device can only be evaluated by the indicator within the device. Therefore, we choose the temperature of the heat source, the temperature rises of the heat source, the final temperature difference between the heat source and the insulator, and the temperature rise ratio between the insulator and heat source as alternative testing indicators.

Fig. 4 (a)-(d) show the temperature of the heat source, the temperature rises of the heat source, the temperature difference between the heat source and the insulator, and the temperature rise ratio between the insulator and the heat source change with heating power and initial temperature after 1 h, respectively. The x and y axes in the figure represent the heating power and initial temperature, respectively, and the z axis represents the temperature of the heat source, the temperature rise of the heat source, the temperature difference between the heat source and the insulator, and the temperature rise ratio between the insulator and the heat source. The red grid plane represents the normal vacuum flask, and the blue grid plane represents the vacuum flask with vacuum failure. Fig. 4(a)–(c) shows that it is not possible to find a cross section (green planes) parallel to the x-y plane to separate the red and blue grid planes completely, indicating that there is not a definite reference value. However, Fig. 4(d) shows that regardless of the changes in heating power and initial temperature, the temperature rise ratios between the insulator and the heat source of the normal and abnormal vacuum flasks are stable at 0.591 and 0.406, respectively. This means that the temperature rise ratio possesses excellent stability. The difference between the temperature rise ratio in the two states is 31.3%, which means that it is significant and distinguishable. The temperature rise ratio planes of normal and abnormal vacuum flasks are completely separated by inserting a plane with a 10% deviation from the normal vacuum flask plane (temperature rise ratio = 0.532) as the critical value, where 10% is the error allowed in industry. These errors may be caused by measurement errors or inadequate evacuation.

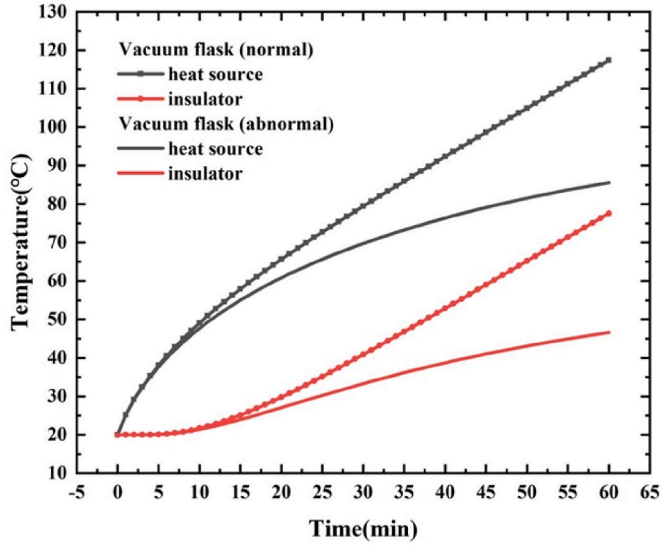

Fig. 3. Temperature curves of the heat source and insulator with an initial temperature of 20 °C and a heat source power of 20 W.

In summary, the temperature rise ratio between the insulator and the heat source satisfies the conditions of the testing indicator. If the test value is less than the critical value Pe, then vacuum failure occurs. The indicator P and critical value Pe can be expressed as:

$$P = \frac{T_M - T_0}{T_1 - T_0} \tag{11}$$

$$Pe = 0.9P \tag{12}$$

where T_0 represents the initial temperature and T_1 and T_M represent the final temperature at the heat source and the insulator, respectively.

After determining the test indicator P, the testing time of the rapid test device needs to be determined. Fig. 5(a) shows the variation in testing indicator P with time. The values of test indicator P in both states show an increasing trend over time. From 20 min to 120 min, the P value of the normal vacuum flask increased from 0.215 to 0.767, while the P value of the abnormal flask increased from 0.173 to 0.475. Fig. 5(b) further shows the curves of the absolute and relative differences in the P value with time for the two states. The absolute and relative differences in P values between the two states increase with time, which means that the longer the testing time is, the more accurately the rapid test device can estimate the vacuum failure. However, it is essential to judge the vacuum failure of the vacuum flask as quickly as possible. Therefore, the testing time is determined to be 1 h, and the absolute and relative differences are 0.186 and 31.39%, respectively, which is enough to judge vacuum failure. The testing time is applied for subsequent numerical simulations and experimental tests.

3. Three-dimensional numerical simulation

3.1. Structure of the rapid test device

Based on the above principles, a rapid test device used to determine vacuum failure of logging tools is designed. Fig. 6 shows the structure of the rapid test device for vacuum failure of the vacuum flask and the structure of the vacuum flask to be tested. The length of the vacuum flask to be tested is 900 mm, with outer and inner diameters of 90 mm and 73 mm, respectively, and the length of the cavity is 847 mm. The vacuum layer of the normal vacuum flask possesses a high vacuum degree, while that of the abnormal one is filled with air, which leads to a tremendous difference in thermal insulation performance. The rapid test device for vacuum failure of the vacuum flask consists of two sections of aluminum alloy shell as well as two insulators with a total length and an outer diameter of 847 mm and 72 mm, respectively, to match the structure of the vacuum flask. The adapter is applied to mount the four heat sources while connected to two sections of the aluminum alloy shell. The shell is a 1.5 mm thick thin-walled pipe to reduce the effect of its own heat capacity on heat transfer. The insulators are made of POM with a low thermal conductivity and a length of 80 mm to reduce heat leakage from the environment. Notably, insulator 1 has a 6 mm hole for

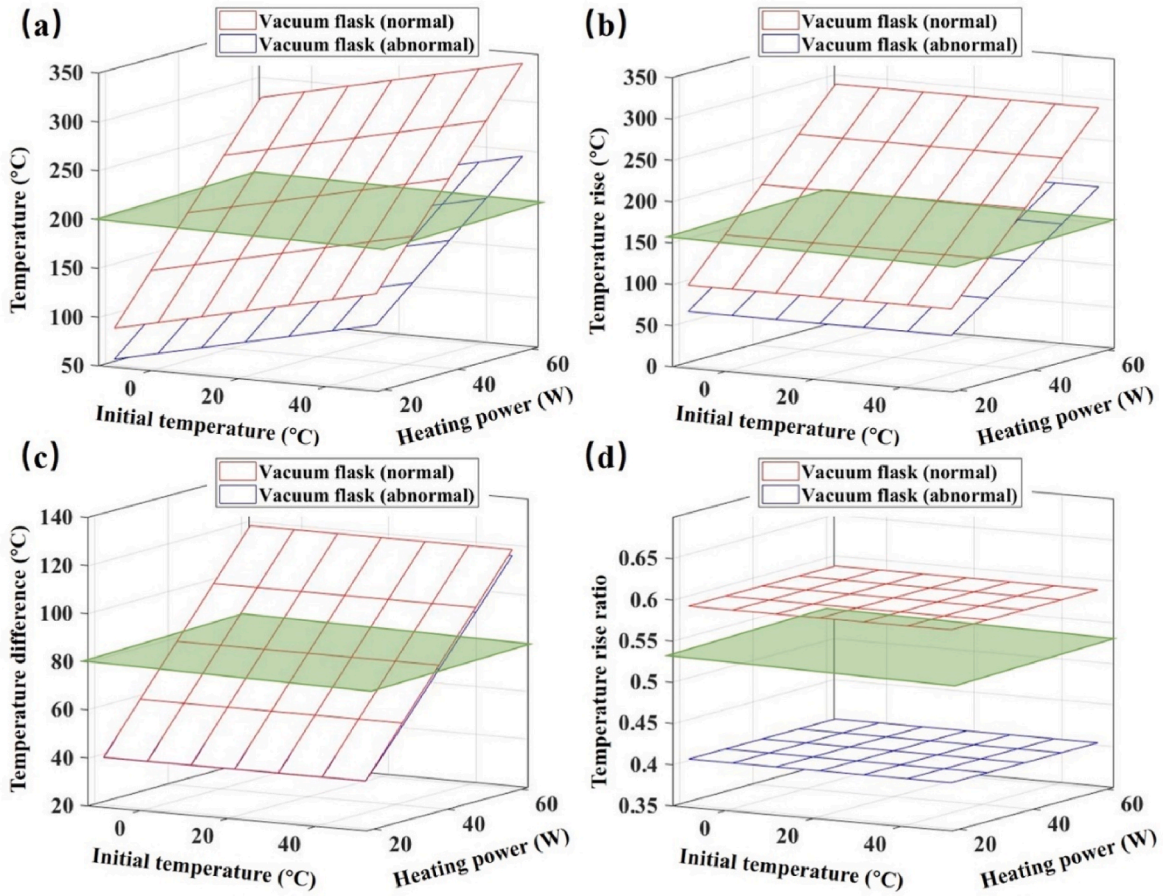

Fig. 4. The alternative testing indicators change with heating power and initial temperature after 1 h. (a) Temperature of the heat source, (b) temperature rise of the heat source, (c) temperature difference between the heat source and the insulator, and (d) temperature rise ratio between the insulator and the heat source.

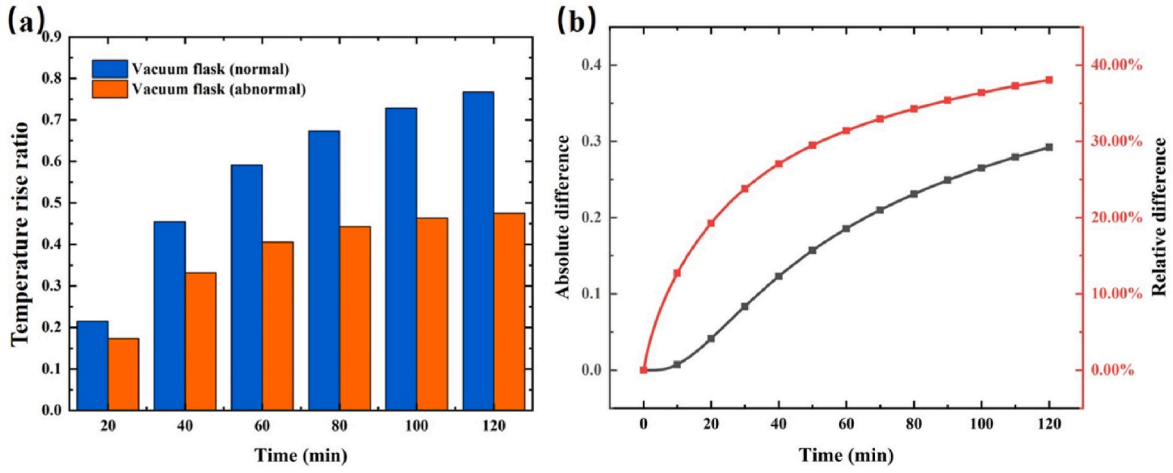

Fig. 5. (a) The variation in test indicator P with time for the two states and (b) the curves of the absolute and relative differences of P values with time for the two states.

the internal heat source and the thermocouple wire.

3.2. Simulation settings

Since the 1D heat transfer model makes many assumptions, 3D numerical simulations are needed to determine the critical value (Pe) of actual vacuum flasks and validate the stability of the testing indicator. To simplify the calculation, some reasonable assumptions are made as follows [23].

(1) The air inside the vacuum flask hardly flows, and natural convective heat transfer is ignored.
(2) Due to the small temperature difference inside the vacuum flask, the radiation heat exchange is ignored.

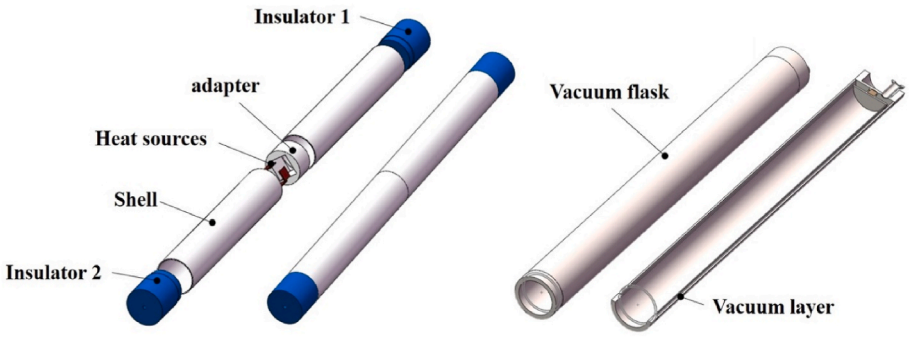

Fig. 6. The structure of the rapid test device for vacuum failure of the vacuum flask of the logging tools and the structure of the vacuum flask to be tested.

(3) The contact thermal resistance between contact surfaces is ignored.
(4) The equivalent thermal conductivity of the vacuum layer is regarded as a solid layer with very low thermal conductivity.

Based on the above assumptions, the heat transfer process of the rapid test device can be simplified to a nonstationary heat conduction model with an internal heat source, which can be expressed as:

$$\rho c \frac{\partial T}{\partial t} = \nabla(\lambda \nabla T) + q \tag{13}$$

where ρ is the material density, c is the constant pressure specific heat capacity of the material, λ is the equivalent thermal conductivity of the material, T is the temperature, and q is the heat source per unit volume.

The software COMSOL was used to perform 3D numerical simulations. The 3D physical model of the rapid test device was imported into the computational fluid dynamics (CFD) solver, and then the free tetrahedral mesh was established. Subsequently, the materials and thermal properties of each component were defined according to Table 1. Notably, the vacuum layer of the normal and abnormal vacuum flasks was equivalent to a solid layer with a thermal conductivity of 0.00014 W/(m·K) and 0.0033 W/(m·K), respectively. To verify the stability of the chosen testing indicator, multigroup simulations with different combinations of parameters for normal and abnormal vacuum flasks were calculated according to Table 2. The heating power of the heat source was defined as 20 W, 30 W, 40 W and 50 W, and the initial temperatures were defined as 20 °C, 30 °C, 40 °C and 50 °C, respectively. Natural convection boundary conditions were used on the outer wall surface of the vacuum flask. The entire heat transfer process was calculated according to a time step of 1 min for 1 h.

To exclude the influence of grid division on the solution results, grid-independence verification was performed. A total of three different grid numbers were set as 40,546, 125,244, and 751,253 grid numbers. The calculated results are shown in Table 3 for an initial temperature of 20 °C and a heating power of 20 W. When the number of grids exceeded 125,244, the temperature variation was small. To save computational resources, a grid number of 125,244 was chosen for the subsequent numerical simulation.

Table 1
Material properties of each component [21].

Name	Material	Thermal conductivity ($W \cdot m^{-1} \cdot K^{-1}$)	Density ($kg \bullet m^{-3}$)	Heat capacity ($J \bullet kg^{-1} \bullet K^{-1}$)
Vacuum bottle	Inconel 718	14.7	8240	436
Vacuum layer	Composite	0.0033/ 0.00014	100	1200
Adapter	Al-6061	167	2710	896
Heat sources	Ceramic	30	3960	850
Insulator	Polyformaldehyde	0.25	2200	1000
Shell	Al-6061	167	2710	896

Table 2
Simulated variables.

Variable Name	List
Equivalent thermal conductivity of vacuum flask/W/(m·K)	0.00014 0.033
Heating power/W	20 30 40 50
Initial temperature/°C	20 30 40 50

Table 3
Grid independent verification.

Grid number	Normal vacuum flask		Abnormal vacuum flask	
	Temperature of insulator/°C	Temperature of heat source/ °C	Temperature of insulator/°C	Temperature of heat source/ °C
40,546	39.080	70.364	30.077	55.835
125,244	40.030	70.924	31.058	56.676
751,253	40.157	71.305	31.056	56.988

4. Experimental validation

Experimental tests were conducted to verify the effectiveness of the rapid test method and the simulated results. Fig. 7 shows a schematic diagram of the experimental test platform, which is composed of a vacuum flask to be tested, a rapid test device, an oven, a DC power supply, thermocouples and a data acquisition instrument. There are two kinds of vacuum flasks: one is the normal state, and the other is the vacuum failure state. The entire rapid test device was loaded into the vacuum flask to be tested. The heat source of the rapid test device consisted of four ceramic heating plates (40 mm × 40 mm × 2 mm, Zhengzhou Xindeng Electrothermal Ceramics Ltd.), powered by a DC

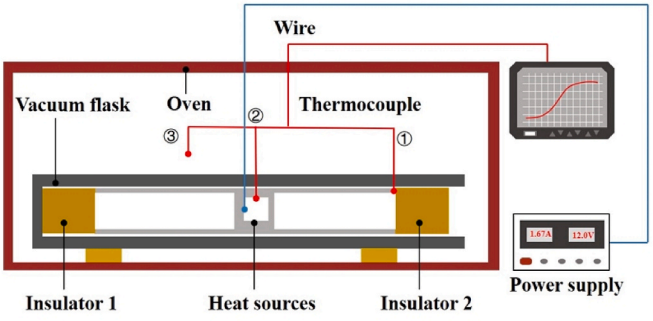

Fig. 7. Schematic diagram of the experimental test platform of the rapid test device.

power supply (MS-3010D, 0–30 V/10 A, Dongguan Meisheng Power Technology Ltd.). Three thermocouples (K type, 2 × 0.3 mm, temperature measurement accuracy = ±0.4 °C) were used to collect the temperature data in the experiment. The temperature measurement points were arranged in the middle of the oven, at the heat source and at the insulator. A data acquisition instrument (MIK-R6000F, temperature measurement accuracy 0.2% FS±1D, sampling frequency = 1 Hz, Hangzhou Mecon Automation Technology Ltd.) was adopted to record and manage the temperature measurement signals. An oven (KH-1000A, temperature range = 10–250 °C, accuracy = ±1 °C, Shanghai Hecheng Instrument Manufacturing Ltd.) was utilized to maintain the set initial temperature, regulated by a proportional–integral–derivative (PID) controller. Fig. 8(a) shows a picture of the total test platform of the rapid test device. Fig. 8(b) displays a picture of the structure of the rapid test device. Note that the four ceramic heating plates were adhered to the adapter by thermal silicone pads (LC120, 1 W/(m·K)). The vacuum flasks to be tested were consistent with the 3D numerical model. One flask was under vacuum, and the other exhibited vacuum failure, as shown in Fig. 8(c). At different powers and different initial temperatures, as shown in Table 4, the rapid test device was applied to test the vacuum flask in the two states for the purpose of verifying the proposed indicator, and each testing time lasted 1 h.

5Results and discussion

5.1. Simulated results

The temperature fields of the two states of the vacuum flask at 60 min were compared by selecting the working conditions at an initial temperature of 20 °C and a heating power of 20 W, as shown in Fig. 9. Fig. 9(a) reflects the temperature field of the normal vacuum flask, and Fig. 9(b) represents the temperature field of the vacuum flask with vacuum failure. From the axial temperature distribution, the temperature in the cavity shows a pattern of high in the middle and low at the two ends, symmetrical with the heat source. On the whole, the temperature inside the cavity of the normal vacuum flask is generally higher than that of the failed vacuum flask. The outer end temperature of the insulator in two vacuum flasks is maintained at the initial temperature, which indicates that the insulator plays the role of preventing the heat from flowing out of the end. In other words, the difference in temperature distribution inside the cavity is mainly caused by circumferential heat leakage. From the radial temperature distribution, the temperature

Table 4
List of experimental variables.

Variable Name	List	
State of vacuum flask	Normal	Abnormal
Heating power/W	20 30 40 50	
Initial temperature/°C	20 30 40 50	

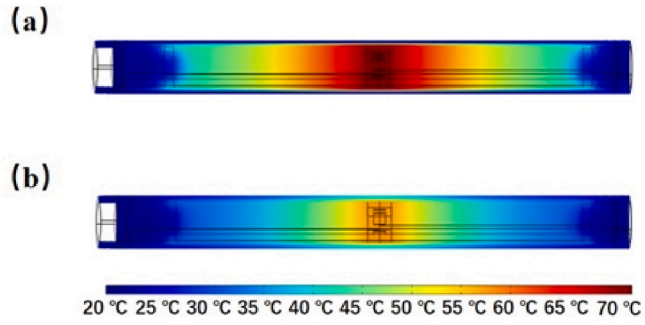

Fig. 9. The temperature field of (a) the normal vacuum flask and (b) the abnormal vacuum flask.

at the heat source in the normal vacuum flask is 72.3 °C, but the outer wall surface remains at approximately the initial 20 °C. In contrast, the temperature at the heat source in the vacuum flask with vacuum failure reaches 58.1 °C, and the temperature of the outer wall surface rises to approximately 38.4 °C. It is easy to conclude that the normal vacuum flask can effectively isolate the heat diffusion between the cavity and the external environment, demonstrating an excellent adiabatic effect. However, after the destruction of the vacuum layer, the adiabatic effect disappears, and the internal heat can easily flow into the external environment through the circumference of the vacuum flask. In summary, the temperature field as a whole reflects the significant difference in the temperature distribution between the vacuum flasks in the two states.

The temperature measurement point of the heat source was selected at the junction of the adapter and the shell, and the temperature measurement point of the insulator was selected at the position of the inside of the insulator parallel to the junction. The values of the testing indicator P in the two states were calculated by using Eq. (11), and the

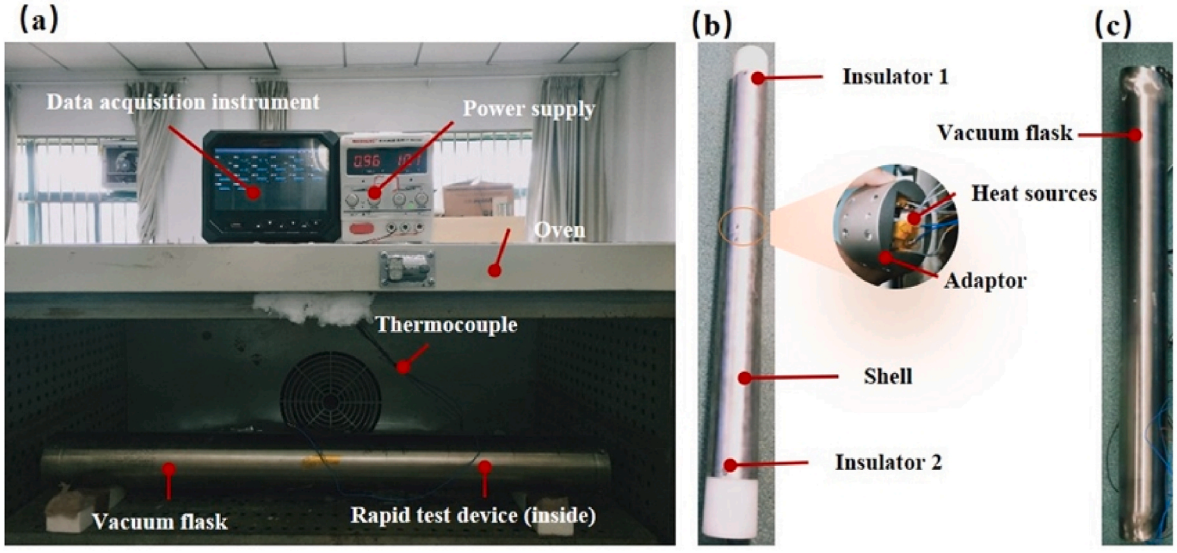

Fig. 8. Photos of the experimental setup: (a) total test platform, (b) rapid test device, and (c) vacuum flask.

critical values Pe were calculated by using Eq. (12). Fig. 10 shows the calculated results of the P values of the two states of the vacuum flask at 60 min for different heating powers and different initial temperatures. The P values of the vacuum flask in the different states vary very little with the heating power and initial temperature, and each is stable at different values. Among them, the P value of the normal vacuum flask is stable at 0.391, and the P value of the vacuum flask with vacuum failure is maintained at 0.299, with a difference of 23.5%. According to the figure, a 10% deviation from the normal vacuum flask plane of the green plane (Pe = 0.351) was selected as the critical value to determine whether the vacuum failure of the vacuum flask to be tested. If $P > 0.351$, then it is determined that the vacuum flask is normal and can be assembled for logging. If $P \leqq 0.351$, then it cannot be guaranteed that the vacuum flask is normal, so a vacuum flask replacement is recommended.

5.2. Experimental results

Fig. 11 shows the experimental results of the rapid test method for vacuum failure of the vacuum flask. The yellow surface is fitted to all groups of experiments for the normal vacuum flask with a mean value of 0.392, and the blue surface is fitted to all groups of experiments for the vacuum failure flask with a mean value of 0.300. The yellow and blue surfaces fluctuate above and below their mean values, and the two surfaces are completely separated. To study the fluctuation of the P value under different conditions, the maximum error between the P value and its average value for each state of the vacuum flask was calculated, as shown in Table 5. Among them, the maximum error value of the normal state is 0.012, and the corresponding error percentage is 3.1%. The maximum error value of the failure state is 0.023, and the corresponding error percentage is 7.7%. This means that the fluctuation of the P value of the vacuum flask in both states is small, and the P value can be regarded as a stable value that does not change with the heating power and initial temperature. In summary, the P value is almost independent of the initial temperature and heating power and only related to the failure of the vacuum layer.

The reason for the fluctuation of the P value in the experiment may come from the following points. Due to the existence of gravity, the rapid test device and the vacuum flask cannot maintain the same axis in the experiments. One side of the rapid test device is in line contact with the inner wall of the vacuum flask, and the other side is slightly farther away from the inner wall of the vacuum flask. Therefore, the heat transfer resistance of the line contact between the side and the vacuum flask is smaller, while the air fills the other side of the gap, resulting in relatively large heat transfer thermal resistance. The temperature measurement point at the heat source is located at the edge of the adapter. Due to inconsistent assembly directions, the temperature measurement points may be located on the side of the larger thermal resistance or the smaller thermal resistance. The fluctuation in the P value of the normal state vacuum flask is smaller since the circumferential thermal resistance of the normal state vacuum flask is large. This suggests that the

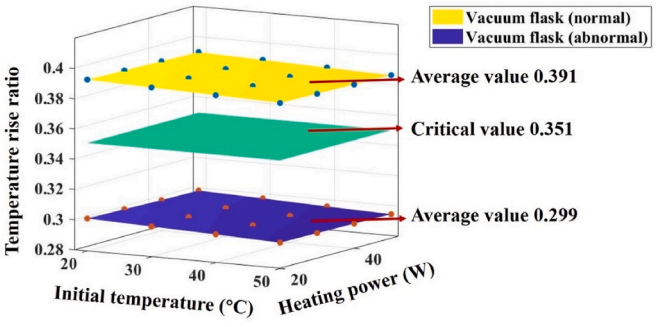

Fig. 10. Calculated results of the P values of the two states of the vacuum flask at 60 min for different heating powers and different initial temperatures.

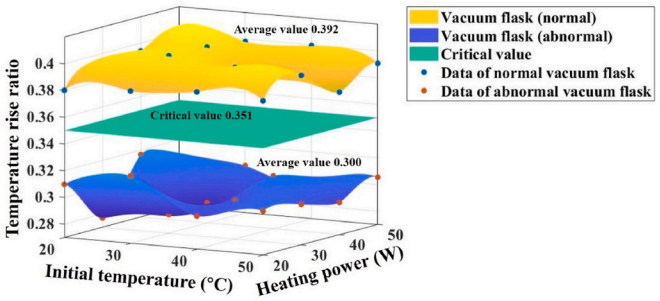

Fig. 11. The experimental test results of the rapid test device for vacuum failure of the vacuum flask.

Table 5
Fluctuation of P under different conditions.

State	Maximum error value	Maximum error value percentage
Normal	0.012	3.1%
Abnormal	0.023	7.7%

unevenness of the circumferential thermal resistance has little influence on it. However, the thermal conductivity of the vacuum layer with vacuum failure is close to air, and the influence of device position eccentricity on its temperature distribution is more obvious, so that the fluctuation of the P value is slightly larger. In addition, the measurement error of the instruments used in the experiment is also a source of error, but the error it produces is smaller.

The P value of the abnormal vacuum flask is 23.5% different from that of the normal vacuum flask, and the distinction is obvious. In Fig. 11, the green surface (Pe = 0.351, calculated by simulations), which is completely independent of the yellow surface and the blue surface, is taken as the critical value to judge whether vacuum failure occurs in the vacuum flask. For the normal vacuum flask, the P value measured under different conditions was greater than the critical value. However, for the vacuum flask with vacuum failure, the P value measured under different conditions is less than the critical value. It can be concluded that the proposed rapid test device can quickly and accurately judge the vacuum failure of a vacuum flask.

5.3. Comparison of experiment and simulation

Fig. 12 compares the simulated results with the experimental results. It can be seen that the experimental values of the two states of the vacuum flask fluctuate up and down. The simulated results and experimental results under the same conditions are compared one by one, and the maximum and average errors are shown in Table 6. For the normal vacuum flask, the maximum error of the P value is only 3.5%, with an average error of only 1.9%. For the abnormal one, the maximum error of the P value reaches 8.7%, with an average error of 3.1%. The error is

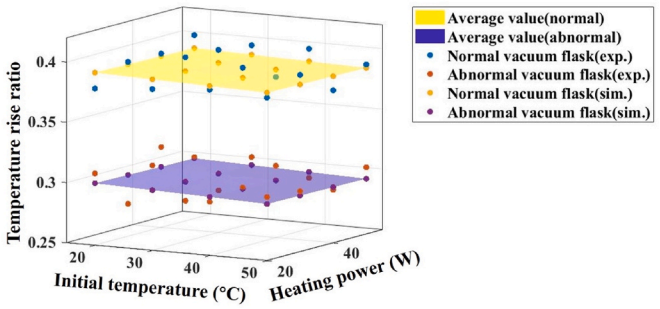

Fig. 12. Comparison of experimental results and simulated results.

Table 6
Experimental and simulated error.

State	Maximum error	Average error
Normal	3.5%	1.9%
Abnormal	8.7%	3.1%

within the acceptable range, thus verifying the accuracy of the simulated results. There are two main reasons for the difference between the simulated and experimental results. On the one hand, the simulated model is established according to the assembly of the two on the same axis, but due to the existence of gravity, the experimental installation of the rapid test device and the vacuum flask to be tested cannot maintain the same axis, which leads to a certain error. Second, due to the limitations of the experimental temperature collection accuracy, measurement errors occur. On the other hand, the effect of interface thermal resistance and the variation in material thermal properties with temperature are ignored in the numerical calculation, and these simplifications also introduce some errors into the simulation.

6Conclusions

To quickly check the vacuum failure of logging tools, a rapid test method based on the variation in equivalent thermal conductivity before and after vacuum failure was proposed in this paper. The calculated results of the 1D heat transfer model showed that the temperature rise ratio between the insulator and heat source (defined as P) can be used as the testing indicator, which does not vary with heating power and initial temperature. The testing time only needs 1 h to judge vacuum failure. Subsequently, a rapid test device was established by the proposed principle, and the stability of the testing indicator was verified at different heating powers and different initial temperatures through 3D numerical simulations. The simulated results showed that the P values for the normal state of the vacuum flask are both 0.391 and that all of the P values for the vacuum failure state are 0.299, with a difference of 23.5%. The critical value (Pe) to determine the failure of the vacuum flask is 0.351. Finally, a prototype was fabricated and experimentally tested. The experimental results showed that under different test conditions, the measured P values of the normal vacuum flask are greater than the critical value, while the measured P values of the abnormal vacuum flask are less than the critical value. This verifies the effectiveness of the rapid test method. Comparing the experimental results with the simulation results, the maximum error is only 8.7%, which verifies the accuracy of the simulated results. It can be concluded that the proposed rapid test method can quickly and accurately judge the vacuum failure of vacuum flasks, which is expected to create massive economic benefits for the oil industry.

Declaration of competing interest

The authors declare that they have no known competing financial interests or personal relationships that could have appeared to influence the work reported in this paper.

Data availability

Data will be made available on request.

Acknowledgment

This research is supported by the National Natural Science Foundation of China (51625601). The authors would like to thank Wei Lan, Yanhua Cheng and Weixian Zhao for their useful discussions.

References

[1] X. Guo, D. Hu, Y. Li, J. Duan, X. Zhang, X. Fan, H. Duan, W. Li, Theoretical progress and key technologies of onshore ultra-deep oil/gas exploration, Engineering 5 (2019) 458–470.
[2] X. Li, X. Jiang, H. Hopman, A review on predicting critical collapse pressure of flexible risers for ultra-deep oil and gas production, Appl. Ocean Res. 80 (2018) 1–10.
[3] N.J. Hyne, Nontechnical Guide to Petroleum Geology, Exploration, Drilling & Production, third ed., PennWell, Tulsa, 2012.
[4] 10-12 A. Shadravan, M. Amani, Hpht 101 - what every engineer or geoscientist should know about high pressure high temperature wells, OnePetro, in: SPE Kuwait International Petroleum Conference and Exhibition. Kuwait City, Kuwait, 2012. SPE-163376-MS.
[5] J. Boyes, The eyes of the oil industry, IEE Rev. 27 (6) (1981) 484–488.
[6] T. Baird, T. Fields, R. Drummond, High-pressure, high-temperature well logging, perforating and testing, Oilfield Rev. 10 (2) (1998) 50–67.
[7] L.T. Yeh, Review of heat transfer technologies in electronic equipment, J. Electron. Mater. 117 (4) (1995) 333–339.
[8] B. Shang, Y. Ma, R. Hu, C. Yuan, J. Hu, X. Luo, Passive thermal management system for downhole electronics in harsh thermal environments, Appl. Therm. Eng. 118 (2017) 593–599.
[9] A. Sinha, Y.K. Joshi, Downhole electronics cooling using a thermoelectric device and heat exchanger arrangement, J. Electron. Packag. 133 (4) (2011), 041005.
[10] B. Holbein, T. Schulenberg, Investigation on refrigerant transport by capillary effect with fleeces in an evaporator for a high temperature cooling machine, Int. J. Refrig. 93 (2018) 18–28.
[11] B. Holbein, J. Isele, L. Spatafora, Cooling systems for borehole tools, Journal of Geological Resource and Engineering 1 (2013) 55–60.
[12] B. Holbein, J. Isele, Development of a cooling system for geothermal borehole probes, Journal of Earth Science and Engineering 4 (2014) 73–79.
[13] A. Sinha, An Adsorption Based Cooling Solution for Electronics Used in Thermally Harsh Environment, Georgia Institute of Technology, Atlanta, 2010.
[14] A. Sinha, Y. Joshi, Application of thermoelectric-adsorption cooler for harsh environment electronics under varying heat load, J. Therm. Sci. Eng. Appl. 2 (2) (2010), 021004.
[15] S. Soprani, J.H.K. Haertel, B.S. Lazarov, O. Sigmund, K. Engelbrecht, A design approach for integrating thermoelectric devices using topology optimization, Appl. Energy 176 (2016) 49–64.
[16] G.A. Bennett, Active Cooling for Downhole Instrumentation: Preliminary Analysis and System Selection, Los Alamos National Laboratory, New Mexico, 1988.
[17] G.A. Bennett, Analytical approach to selecting and designing a miniature downhole refrigerator, J. Energy Resour. Technol. 114 (4) (1992) 339–344.
[18] W. Gao, K. Liu, H. Jia, D. Hong, X. Teng, Challenge of temperature control for downhole instruments in HTHP reservoir, in: SPE Offshore Europe Conference and Exhibition, Aberdeen, OnePetro, 2019, 195712. UK, 3-6 Sept. 2019.
[19] W. Gao, K. Liu, X. Dou, S. Tang, L. Zhang, Numerical investigation on cooling effect in the circuit cabin of active cooling system of measurement-while-drilling instrument based on split-Stirling refrigerator, Case Stud. Therm. Eng. 28 (2021), 101621.
[20] W. Gao, K. Liu, X. Dou, L. Zhang, S. Tang, Numerical investigation on heat transfer rate from the outside environment into the electronic compartment of the measurement-while-drilling tools, Heat Transfer 50 (6) (2021) 5835–5852.
[21] W. Lan, J. Zhang, J. Peng, Y. Ma, S. Zhou, X. Luo, Distributed thermal management system for downhole electronics at high temperature, Appl. Therm. Eng. 180 (2020), 115853.
[22] J. Zhang, W. Lan, C. Deng, F. Wei, X. Luo, Thermal optimization of high-temperature downhole electronic devices, IEEE Trans. Compon. Packag. Manuf. Technol. 11 (2021) 1816–1823.
[23] Y. Ma, B. Shang, R. Hu, X. Luo, Thermal management of downhole electronics cooling in oil & gas well logging at high temperature, in: 17th International Conference on Electronic Packaging Technology, 2016, pp. 623–627.
[24] S. Rafie, Thermal management of downhole oil & gas logging sensors for hthp applications using nanoporous materials, Proceedings of 2nd Energy Nanotechnology International Conference 81 (2007) S910–S931.
[25] J. He, Q. Wang, J. Wu, Y. Zhang, W. Chu, Hybrid thermal management strategy with PCM and insulation materials for pulsed-power source controller in extreme oil-well thermal environment, Appl. Therm. Eng. 214 (2022), 118864.
[26] J. Peng, W. Lan, Y. Wang, Y. Ma, X. Luo, Thermal management of the high-power electronics in high temperature downhole environment, in: 2020 IEEE 22nd Electronics Packaging Technology Conference, EPTC), 2021, pp. 369–375.
[27] E. Pennewitz, M. Schilling, T. Kruspe, S. Jung, A. Ruehs, Active cooling of downhole instrumentation for drilling in deep geothermal reservoirs, in: IEEE Instrumentation and Measurement Technology Conference, 2012, pp. 600–603.
[28] J.A. Demko, R.C. Duckworth, M. Roden, M. Gouge, Testing of a vacuum insulated flexible line with flowing liquid nitrogen during the loss of insulating vacuum, Adv. Cryog. Eng. 53A (2008) 160–167.
[29] V.D. Bartenev, V.I. Datskov, Y.A. Shishov, A.G. Zel Dovich, Study of the processes of insulation vacuum failure in helium cryostats, Cryogenics 26 (5) (2012) 293–296.
[30] G.F. Xie, X.D. Li, R.S. Wang, Study on the heat transfer of high-vacuum-multilayer-insulation tank after sudden, catastrophic loss of insulating vacuum, Cryogenics 50 (10) (2010) 682–687.
[31] K.O. Pomeroy, M.L. Reed, B. LoManto, S.G. Harris, W.B. Hazelrigg, D.A. Kelk, Cryostorage tank failures: temperature and volume loss over time after induced

failure by removal of insulative vacuum, J. Assist. Reprod. Genet. 36 (11) (2019) 2271–2278.
[32] M. Zhu, R.S. Wang, Study on the heat transfer of complex-vacuum-multilayer-insulation tank after sudden loss of insulation vacuum, Heat Mass Tran. 48 (11) (2012) 1881–1887.
[33] X. Han, G. Li, M. Xu, C. Guo, Y. Wang, Y. Feng, D. Li, Miniature capacitance diaphragm gauge for absolute vacuum measurement, Measurement 194 (2022), 110851.
[34] J.M. Jurns, G.M. Pease, R.R. Tison, R.J. Sprafka, R.F. Nigro, Testing of a buried LNG tank, Adv. Cryog. Eng. 43 (1998) 1215–1221.
[35] W. Wei, X. Li, R. Wang, L. Yang, Effects of structure and shape on thermal performance of perforated multi-layer insulation blankets, Appl. Therm. Eng. 29 (5–6) (2009) 1264–1266.
[36] B. Wang, R. Luo, H. Chen, C. Zheng, Y. Gao, H. Wang, A.R. Hashmi, Q. Zhao, Z. Gan, Characterization and monitoring of vacuum pressure of tank containers with multilayer insulation for cryogenic clean fuels storage and transportation, Appl. Therm. Eng. 187 (2021), 116569.
[37] Y. Huang, B. Wang, S. Zhou, J. Wu, G. Lei, P. Li, P. Sun, Modeling and experimental study on combination of foam and variable density multilayer insulation for cryogen storage, Energy 123 (2017) 487–498.
[38] G.E. McIntosh, Layer by layer MLI calculation using a separated mode equation, Adv. Cryog. Eng. 39 (1994) 1683–1690.
[39] J.P. Holman, Heat Transfer, tenth ed., McGraw Hill Education, New York, 2009.